J|A|C|S
ARTICLES
Published on Web 02/03/2005

Multiply Doped Nanostructured Silicate Sol−Gel Thin Films: Spatial Segregation of Dopants, Energy Transfer, and Distance Measurements

Payam N. Minoofar,[†] Bruce S. Dunn,[‡] and Jeffrey I. Zink*,[†]

Contribution from the Departments of Chemistry and Biochemistry and of Materials Science and Engineering, University of California, Los Angeles, California 90095

Received August 9, 2004; E-mail: zink@chem.ucla.edu

Abstract: Physical and chemical strategies that place designed molecules in spatially separated regions of surfactant-templated mesostructured silicate thin films are used to prepare films containing rhodamine 6G (R6G), lanthanide complexes, and both simultaneously. Fluorescence and photoexcitation spectra of R6G in amorphous and structured thin films show that it is located inside the surfactant micelles of structured thin films. A silylated ligand that binds lanthanides condenses to form part of the silica framework and causes the lanthanide to localize in the silica. Luminescence and photoexcitation spectra show that energy transfer from the metal complex to R6G occurs in the films. R6G quenches Tb emission in a concentration-dependent manner. Energy transfer efficiency is calculated using the Tb luminescence lifetime, and this quantity is used to calculate the distance between Tb and R6G with the aid of Förster theory.

Introduction

Surfactant-directed self-assembly of nanosize pores in silica thin films is increasingly being used to make photoresponsive materials.[1−15] We recently developed one-step, one-pot synthetic strategies to place deliberately photoactive molecules in spatially separated regions.[5,13,15] These regions are defined as the silicate matrix, the hydrophobic core of surfactant micelles, and the intervening ionic interface between surfactant headgroups and the silica framework. In this approach, all of the components including the photoactive species and the structure-directing agents are dissolved in the starting sol. Dip coating of this sol onto a substrate produces doped mesostructured films. The earliest examples used luminescent molecules that were designed to probe the film formation.[4,6−8,16] The micelle assembly process was monitored and correlated with changes in solvent composition. Probes that were preferentially incorporated in specific regions (such as the micelle interior) were chosen. In the most recent examples, designed placement of two or more molecules has been demonstrated.[13]

Doping can be performed during synthesis[9,17−20] as described above or after the film synthesis is complete. Postsynthesis doping involves surfactant removal (if surfactant templates are used) followed by immersion of the material in a solution containing the dopant.[14] This back-filling step affords a high degree of control over the final location of the dopant by targeting the pores, but dopant loads achieved this way are low because diffusion is slow and because not all pores may be accessible. The inner surface of the pores may require chemical modification after surfactant removal to accept the dopant. By having the luminescent dopants present in the precursor sol, higher concentrations may be incorporated uniformly into the final material.

The silicate thin films used in the studies reported in this paper are templated by the ionic surfactant cetyltrimethylammonium bromide (CTAB). The mesostructure and the three regions are depicted in Figure 1. Luminescent molecules

[†] Department of Chemistry and Biochemistry.
[‡] Department of Materials Science and Engineering.

(1) Lu, Y. F.; Ganguli, R.; Drewien, C. A.; Anderson, M. T.; Brinker, C. J.; Gong, W. L.; Guo, Y. X.; Soyez, H.; Dunn, B.; Huang, M. H.; Zink, J. I. *Nature* **1997**, *389*, 364−368.
(2) Huang, M. H.; Kartono, F.; Dunn, B.; Zink, J. I. *Chem. Mater.* **2002**, *14*, 5153−5162.
(3) Liu, N.; Dunphy, D. R.; Atanassov, P.; Bunge, S. D.; Chen, Z.; Lopez, G. P.; boyle, T. J.; Brinker, C. J. *Nano Lett.* **2004**, *4*, 551−554.
(4) Huang, M. H.; Soyez, H. M.; Dunn, B. S.; Zink, J. I. *Chem. Mater.* **2000**, *12*, 231−235.
(5) Hernandez, R.; Franville, A.; Minoofar, P.; Dunn, B.; Zink, J. *J. Am. Chem. Soc.* **2001**, *123*, 1248−1249.
(6) Franville, A. C.; Dunn, B.; Zink, J. I. *J. Phys. Chem. B* **2001**, *105*, 10335−10339.
(7) Huang, M. H.; Dunn, B. S.; Zink, J. I. *J. Am. Chem. Soc.* **2000**, *122*, 3739−3745.
(8) Huang, M. H.; Dunn, B. S.; Soyez, H.; Zink, J. I. *Langmuir* **1998**, *14*, 7331−7333.
(9) Wirnsberger, G.; Yang, P.; Huang, H.; Scott, B.; Deng, T.; Whitesides, G.; Chmelka, B.; Stucky, G. *J. Phys. Chem. B* **2001**, *105*, 6307−6313.
(10) Valverde, G.; Macedo, J. G.; Cruz, D.; Zink, J. I.; Hernandez, R. *J. Sol-Gel Sci. Technol.* **2003**, *26*, 605−608.
(11) Li, H. R.; Fu, L. S.; Lin, J.; Zhang, H. J. *Thin Solid Films* **2002**, *416*, 197−200.
(12) Hernandez, R.; Tseng, H.-R.; Wong, J. W.; Stoddart, J. F.; Zink, J. I. *J. Am. Chem. Soc.* **2004**, *126*, 3370−3371.
(13) Minoofar, P.; Franville, A.; Chia, S.; Hernandez, R.; Dunn, B.; Zink, J. *J. Am. Chem. Soc.* **2002**, *124*, 14388−14396.
(14) Nguyen, T.-Q.; Wu, J.; Doan, V.; Tolbert, S. H.; Schwartz, B. J. *Science* **2000**, *288*, 652−656.
(15) Minoofar, P.; Hernandez, R.; Franville, A. C.; Chia, S. Y.; Dunn, B.; Zink, J. I. *J. Sol-Gel Sci. Technol.* **2003**, *26*, 571−575.
(16) Soyez, H.; Huang, M.; Dunn, B.; Zink, J. I. *Proc. SPIE-Int. Soc. Opt. Eng.* **1997**, *3136*, 118−126.
(17) Bekiari, V.; Ferrer, M.-L.; Lianos, P. *J. Phys. Chem. B* **1999**, *103*, 9085−9089.
(18) Lam, K. S.; Lo, D. *Appl. Phys. B* **1998**, *66*, 427−430.
(19) Nishikiori, H.; Fujii, T. *J. Phys. Chem. B* **1997**, *101*, 3680−3687.
(20) Wirnsberger, G.; Scott, B. J.; Stucky, G. D. *Chem. Mater.* **2001**, *13*, 3140−3150.

 10.1021/ja045185e CCC: $30.25

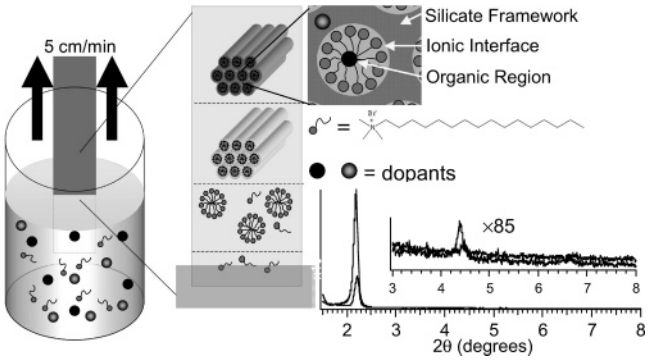

Figure 1. Sketch of the film pulling process (left), the evolution of the mesostructured film with time (middle), the three regions of mesostructured thin films templated by an ionic surfactant (right), and representative X-ray diffraction patterns of the nanopatterned thin films. The structures of the luminescent dopants are shown in Charts 1 and 2.

containing three or more condensable alkoxysilane groups that cocondense with the silicate precursor are chemically bonded in the silicate framework, and organic dyes associate with the hydrophobic organic region of the surfactant template.

In this paper we report the preparation of thin films simultaneously doped with two different luminescent molecules located in two different spatially separated regions.[13] The molecules are chosen for use in quantitative studies of energy transfer between the nanoscaled regions. Luminescence spectroscopy shows that rhodamine 6G (R6G), the molecule chosen as the energy acceptor, is incorporated into the surfactant micelles and that lanthanide (specifically Eu and Tb) complexes chelated by the alkoxysilylated ligand shown in Chart 1 are incorporated into the silicate framework. When the lanthanide's ligand is not silylated, the complex is incorporated in the surfactant region of the structured film. Quantitative measurements of energy transfer between Tb and R6G in the mesostructured films are made and used to calculate the distance between the donor and acceptor. Steady-state fluorescence and photoexcitation spectra and R6G and the Tb complex's luminescence lifetimes show that excited Tb complexes transfer their energy to R6G molecules in a concentration-dependent manner. The excitation spectra show that absorption of light by the lanthanide complex results in emission of light from the R6G. The lifetime of the lanthanide complex decreases, and that of R6G increases. Förster theory is used to calculate the separation between Tb and R6G. At high R6G (acceptor) concentrations the distance approaches 29 ± 5 Å.

Experimental Section

General Sol Preparation and Film Synthesis. Films are synthesized as described previously.[1,13] First, a stock solution is prepared by mixing tetraethoxysilane (TEOS, the silicate precursor), ethanol, water, and HCl with mole ratios 1:3.8:1:(5×10^{-5}), respectively, and refluxing at 60 °C for 90 min. A 7.5 mL sample of this stock solution is then mixed with 0.9 mL of 0.07 M HCl and 0.3 mL of water in a Nalgene plastic beaker, and the resulting solution is stirred for 15 min and then aged for 15 min. At this point 19 mL of absolute ethanol is added to the mixture to make the sol. A strip of silicon, cleaned with piranha solution (H_2O_2/H_2SO_4, 1:4 by volume, heated to nearly boiling for 1 h), is dipped into a Teflon reservoir containing the sol and withdrawn at a constant rate between 5 and 10 cm/min to yield an amorphous film. The sol is then transferred back to the beaker, and 0.76 g of CTAB (3.5% by mass) is dissolved in the sol with a minimum of 10 min of vigorous stirring. A second film is then dip coated onto a silicon strip to yield a mesostructured film. The entire film pulling apparatus is contained inside a controlled humidity chamber, and all films are prepared at a relative humidity of 60 ± 5%.

Preparation of Films Containing R6G. Laser-grade rhodamine 6G (99%) was purchased from Aldrich Chemicals (St. Louis, MO) and used as received. R6G was added to the final sol and dissolved completely after a minimum of 5 min of stirring. Two films were pulled from each sol, one before the addition CTAB and one after. Films were prepared from sols with R6G:CTAB mole ratios of 1:1000, 15:1000, 24:1000, 36:1000, and 50:1000 by varying the R6G content.

Preparation of Films Containing Pyridinedicarboxylic Acid and Europium. This Eu complex is shown in Chart 2. Pyridinedicarboxylic acid (PyDCA) and europium trichloride hexahydrate were purchased from Aldrich Chemicals (St. Louis, MO) and used as received. The amount of $EuCl_3 \cdot 6H_2O$ required by the desired PyDCA:Eu mole ratio was dissolved in the first step of the sol preparation when the solution is most acidic. After the final sol was obtained, 60 mg of PyDCA, Si:PyDCA = 550:100, was added to the sol and two films were withdrawn as described above: one before the addition of CTAB and one after.

Chart 1

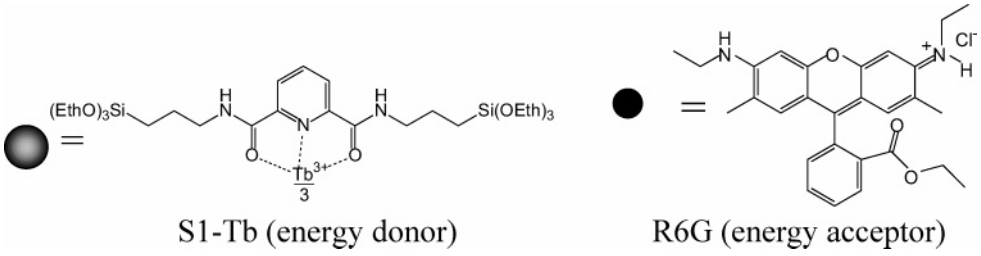

Chart 2

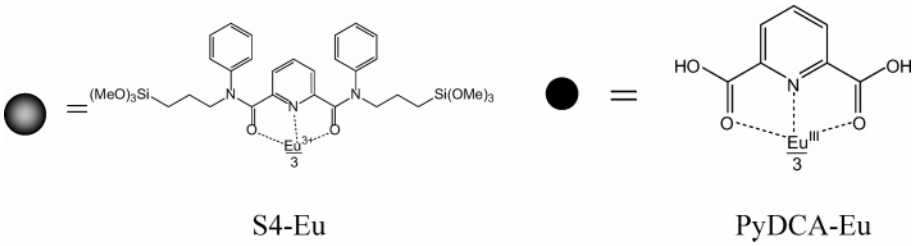

Preparation of Films Containing Europium and the Silylated Ligand S4. The S4 ligand, shown in Chart 2, was synthesized according to a published method.[21] Upon isolation, 2.5 g of the ligand was dissolved in 80 mL of the stock solution, and this stock solution was used to prepare thin films containing the silylated ligand. As with PyDCA−Eu films described above, the chloride salt of Eu was dissolved in the first step of the sol preparation, and two different films were prepared: one before the addition of CTAB and one after the dissolution of 3.5% of the mass of CTAB (0.76 g). The Si:S4 mole ratio used in the studies in this paper was 50:1, and the Eu:S4 ratios were 1:6 and 2:3.

Preparation of Films Containing Tb and R6G. These films were prepared by dissolving $TbCl_3$ and R6G in a sol containing the S1 ligand. First, the S1 ligand (Chart 1) was prepared according to a previously described method.[21] The product, 2.6 g, was dissolved in the stock solution. The total volume of this spiked stock solution was 71 mL, and the S1 concentration was 0.063 M (Si:S1 = 39:1). Then, 61 mg of $TbCl_3 \cdot 6H_2O$ (Aldrich Chemicals), S1:Tb = 3:1, was dissolved during the first step of the sol preparation when the solution is most acidic. Once the final sol was ready, three films were pulled onto silicon substrates. The first film contained S1−Tb only. Then, the required amount of R6G was dissolved in the sol, and the second film was pulled. Then, 0.76 g of CTAB was dissolved in the sol, and the third film was pulled from the sol. Four sets of films were prepared at R6G:Tb ratios of 1.6:100, 6.7:100, 20:100, and 50:100, at fixed S1−Tb concentration. Each set of films consists of an amorphous film containing S1−Tb only, an amorphous film containing S1−Tb and R6G, and a mesostructured film containing S1−Tb and R6G.

Instrumentation and Analysis. X-ray diffraction patterns were obtained on a locally constructed powder diffractometer that uses the 1.5418 Å Cu Kα line. UV−vis absorption spectra were obtained on a Shimadzu UV3101-PC scanning spectrophotometer over the wavelength range 200−800 nm. Steady-state luminescence and luminescence excitation spectra were obtained on either a Spex model 1902 Fluorolog or a Jobin-Yvon-Spex Tau3 Fluorolog spectrofluorometer. Excitation for luminescence spectra was at 300 nm and also at 530 nm in films containing R6G only. The R6G luminescence peak at 560 nm was monitored to generate the photoexcitation spectra of R6G in films that contained R6G only. Tb excitation spectra were obtained by monitoring the 545 nm Tb luminescence line in films that contained Tb only. In films containing both Tb and R6G, R6G fluorescence at 575 nm (where Tb luminescence is not detectable) was monitored to generate the photoexcitation spectra.

Frequency domain (FD) fluorescence lifetime[22] data for R6G fluorescence lifetimes were obtained on the Tau3 Fluorolog spectrofluorometer. The range of modulation frequencies available from this instrument is 0.1−300 MHz, and luminescence lifetimes between 10 μs and 10 ps can be measured. Because modulating the exciting light severely attenuates its intensity, the majority of the R6G emission envelope (light that passed a 550 or 570 nm cutoff filter) was captured for this analysis. In films containing R6G but no Tb, modulation was varied from 10 to 130 MHz and excitation was either at 530 nm or at 330 nm. For the films with both R6G and Tb, excitation was at 330 nm (where the Tb ligand absorbs) and the modulation was varied from 1 to 130 MHz. A total of 10−15 points were collected in each experiment, and the results were modeled with the curve fitting package (Galactic) that was supplied with the instrument. Constant standard deviations of 0.5 and 0.005 for the phase shift and the modulation data, respectively, were used in modeling the lifetimes. Using constant error rates yields more consistent lifetimes.[22]

Ln luminescence lifetimes were obtained by exciting each sample with a 20 ns 266 nm laser pulse and monitoring the emission. The excitation source was a Quantel Brilliant Nd:YAG laser with a repetition rate of 20 Hz. The film luminescence was passed through a single monochromator that disperses the light onto a Roper Scientific PI-MAX gated, intensified CCD camera system. The camera was programmed to collect 150 spectra over each of the following time ranges: 1 ns to 4 ms, 1 ns to 2 ms, and 1 ns to 50 μs. Over any given time range, the time interval over which spectra were collected was approximately 75% of the time increment between points. For example, when the time increment separating points was 0.027 ms, spectra were collected for 0.02 ms at each time point. Twenty spectra were accumulated at each time point to increase the signal-to-noise ratio. The data sets were then exported as two-dimensional arrays (733 pixels on the camera by 150 time points) to the data analysis program Igor Pro.

Igor Pro was used to visualize the decay spectra, to construct decay curves, and to fit the decay curves. The decay curves were generated by summing the intensities for the points comprising each peak at each time point and reporting that sum as the intensity at that particular time point. These sums were calculated for each lanthanide peak. For R6G, decay curves were obtained from the range 558−572 nm (the region between the Tb 545 and 585 nm peaks for which no Tb intensity was observed). Decays were described as sums of exponentials:

$$I(t) = C + \sum A_i \exp\left(-\frac{t}{\tau_i}\right) \quad (1)$$

Fits to sums of more than two exponentials are reported only when they simultaneously reduced the χ^2 value by more than 50% and yielded more randomly distributed residuals relative to expressions with fewer exponential terms.

A weighted average lifetime was calculated for each decay according to

$$\langle\tau\rangle = \sum \alpha_i \tau_i \quad (2)$$

where

$$\alpha_i = \frac{A_i \tau_i}{\sum A_i \tau_i} \quad (3)$$

and A_i are the preexponential factors returned by the fitting algorithm when decay curves are fit to eq 1.

Results

1. Mesostructure. X-ray diffraction patterns of thin films obtained from the above syntheses are shown in Figure 1. Patterns from films lacking CTAB contained no peaks. All films containing CTAB showed the same diffraction pattern, regardless of the dopant concentration. The first-order diffraction peak appears at $2\theta = 2.22° \pm 0.05°$, and a weak second-order diffraction peak appears at $2\theta = 4.45° \pm 0.05°$, corresponding to a lattice spacing of 39.8 ± 0.7 Å.

2. Spectra and Luminescence Lifetimes.

A. Rhodamine 6G. Steady-state fluorescence and fluorescence excitation spectra of films containing R6G are shown in Figure 2. The top panel compares the fluorescence and fluorescence excitation spectra collected from mesostructured thin films with the spectra obtained from amorphous films. For films obtained at an R6G:CTAB mole ratio of 15:1000 in the precursor sol, the fluorescence peak of the mesostructured film is 27 times more intense than that of the amorphous film, and the excitation peak intensity of the mesostructured film is 42 times more intense than the excitation peak of the amorphous film. More intense spectra were obtained from mesostructured

(21) Franville, A. C.; Zambon, D.; Mahiou, R.; Chou, S.; Troin, Y.; Cousseins, J. C. *J. Alloys Compd.* **1998**, *277*, 831−834.
(22) Lakowicz, J. R. *Principles of Fluorescence Spectroscopy*, 2nd ed.; Kluwer Academic: New York, 1999.

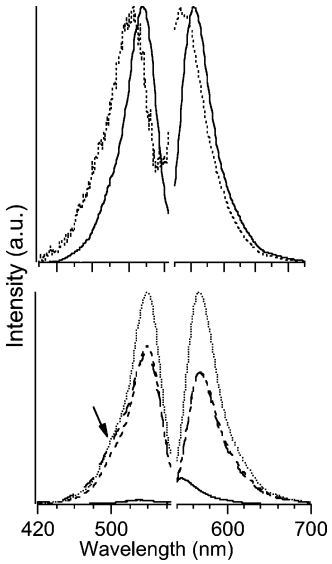

Figure 2. Fluorescence and excitation spectra of thin films containing different concentrations of R6G. (Top) Excitation (left) and emission spectra collected from amorphous films (dotted line) and mesostructured films (solid line) containing R6G at R6G:CTAB = 15:1000. The excitation spectrum and the fluorescence spectrum of the amorphous film have been magnified 42× and 27×, respectively. The excitation and fluorescence maxima of R6G in structured films are red shifted 7 and 14 nm, respectively, relative to the same maxima for R6G in amorphous films. (Bottom) Emission and excitation spectra from mesostructured films at the R6G:CTAB ratios 1:1000 (solid line), 24:1000 (dotted line, most intense spectra), 34:1000 (broken line), and 50:1000 (dashed line). The R6G fluorescence intensity decreases for R6G:CTAB ratios higher than 24:1000. The arrow points to the shoulder that has been attributed to R6G aggregates in absorption spectra.

Table 1. R6G Lifetimes in Mesostructured Thin Films[a]

R6G:CTAB[b]	% $\tau_1 \pm 5$	$\tau_1 \pm 0.5$ (ns)	% $\tau_2 \pm 5$	$\tau_2 \pm 0.5$ (ns)	% $\tau_3 \pm 5$	τ_3 (ns)
1:1000[c]	75	3	20	0.4	5	140
15:1000	95	2			5	12
24:1000	60	2	30	0.8	10	10
34:1000	30	2	62	0.3	8	8
50:1000	26	4	70	0.7	4	54

[a] Lifetime percentages are calculated according to eq 3. The subnanosecond lifetimes reported are equal within the experimental error. The errors reported are estimated on the basis of multiple measurements. Reference 12 provides a thorough review of how the rate law is obtained in FD lifetime measurements. [b] Ratios of the molecules in the sol. [c] The error associated with this measurement was larger because the signal was low.

films at all R6G concentrations. The ratio of the intensity from a mesostructured film to the intensity from the corresponding amorphous film ranged from 5 to 20. In all instances the R6G peak maximum (for both fluorescence and excitation) from the mesostructured film is red shifted by 2−10 nm relative to the corresponding peak from the amorphous film. The bottom panel of Figure 2 compares the intensities of R6G in mesostructured films at different R6G:CTAB mole ratios (based on amounts added to the precursor sol). As more R6G is added, the R6G fluorescence intensity increases, but at R6G:CTAB ratios higher than 24:1000, the R6G fluorescence intensity decreases.

Lifetimes obtained from modeling modulation and phase-shift data obtained from films with R6G are summarized in Table 1. R6G is excited at 530 nm. At the lowest R6G concentration, the lifetime is dominated by a 2 ns lifetime component that comprises more than 75% of the overall lifetime. When the concentration of R6G exceeds an R6G:CTAB ratio of 24:1000, a subnanosecond lifetime component appears. This fast lifetime component grows and dominates the overall decay law at an R6G:CTAB ratio of 50:1000.

Table 2. Dependence of Europium 616 nm Luminescence Lifetimes on the Ligand and Environment[a]

ligand	Ln:ligand	type	% τ_1	τ_1 (ms)	% τ_2	τ_2 (ms)
PyDCA	1:3	amorphous	98.2	0.77	1.8	0.03
		structured	97.9	0.95	2.9	0.06
	2:3	amorphous	100	0.39		
		structured	93.5	0.47	6.5	0.06
S4	1:6	amorphous	82.7	0.56	17.3	0.15
		structured	83.0	0.61	17.0	0.15
	2:3	amorphous	46.2	0.61	50.8	0.22
					3.0	0.03
		structured	73.6	0.62	26.4	0.24

[a] The lifetime percentages are calculated according to eq 3. Standard deviations for lifetime percentages and lifetimes are $\sigma \leq 5\%$.

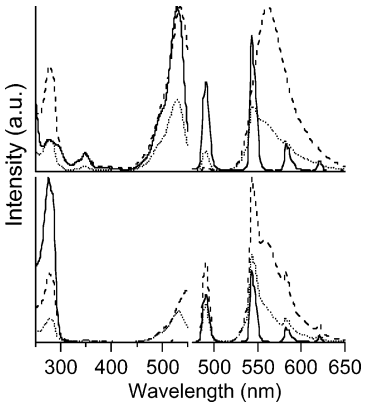

Figure 3. Absorption spectrum of R6G (ethanol solution, left side), emission spectra (right side), and photoexcitation spectra (left side) from S1−Tb−R6G films at R6G:Tb = 6.7:100 (top) and 1.6:100 (bottom). Emission spectra are from amorphous films containing S1−Tb only (solid line), amorphous films with both S1−Tb and R6G (dotted line), and structured films with S1−Tb and R6G (dashed line). The excitation spectra are similarly rendered with the following exceptions: the solid trace in the top left panel is the absorption spectrum of an ethanol solution of R6G, and the solid trace in the bottom left panel is the excitation spectrum of the S1−Tb complex obtained from the amorphous film whose emission spectrum appears to its right. The R6G absorption maximum matches the R6G excitation maximum in an amorphous film.

B. Lanthanide Complexes. Steady-state luminescence spectra show the typical emission lines of the incorporated lanthanide. Luminescence excitation spectra verify lanthanide sensitization by the ligand, as the shapes of the excitation profiles and their maxima match those of the absorption spectra of the ligands exactly.

When pyridinedicarboxylic acid is used as the ligand, Eu luminescence lifetimes in structured films are on average 10% longer than lifetimes from the corresponding amorphous films (Table 2). There is a nearly 50% drop in the Eu luminescence lifetime when the Eu:PyDCA concentration ratio is reduced to 2:3 from 1:3. When Eu is bound to S4, shorter lifetimes are obtained, but the lifetimes in structured films are about the same as those obtained from amorphous films, regardless of the S4:Eu ratio.

C. Tb−R6G Films. Steady-state luminescence and luminescence excitation spectra of films containing S1−Tb and R6G are shown in Figure 3. The luminescence spectra obtained with 300 nm excitation show that, as the R6G concentration increases, the Tb luminescence intensity decreases. R6G emission in these films is more intense than the emission obtained from similar

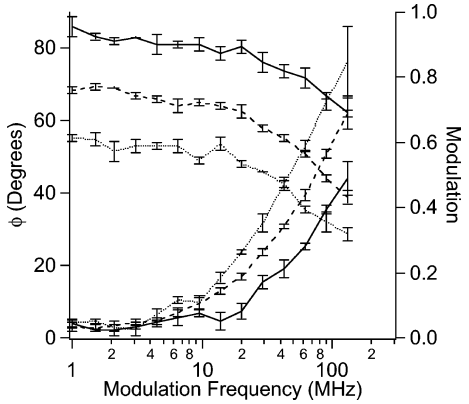

Figure 4. Phase shift and modulation curves used to calculate R6G lifetimes in mesostructured films with S1−Tb and R6G at R6G:Tb ratios of 50:100 (solid line), 20:100 (dashed line), and 6.7:100 (dotted line). At Tb:R6G = 50:100, phase shift and modulation traces do not cross. Hence, aggregates dominate at this R6G content. Also, the long lifetime component is not a significant component of the overall lifetime, consistent with rapid and complete quenching expected at low donor:acceptor ratios. At R6G:Tb = 6.7:100, the long lifetime is a majority component of the overall R6G lifetime as seen in the very low modulation (55%) at the lowest frequency of modulation of exciting light (1 MHz). This result is consistent with moderate quenching at high donor:acceptor ratios.

Table 3. Lengthening of R6G Lifetimes as a Result of Energy Transfer from Tb in Mesostructured Thin Films

R6G:Tb	% $\tau_1 \pm 5$	$\tau_1 \pm 0.5$ (ns)	% $\tau_2 \pm 5$	$\tau_2 \pm 200$ (ns)	% $\tau_3 \pm 5$	$\tau_3 \pm 5$ (ns)
6.7:100	68	2	28	1550	4	64
20:100	60	2	28	846	12	10
50:100	63	1	12	258	25	5

[a] Lifetime percentages were calculated according to eq 3. The errors reported are based on multiple measurements.

films without Tb. The R6G excitation spectra obtained from the films containing both R6G and S1−Tb show a new peak in the UV region at the S1−Tb excitation maximum.

R6G fluorescence lifetimes (calculated from fits to experimentally obtained modulation and phase shift curves depicted in Figure 4) obtained from films with varying ratios of the S1−Tb complex to R6G are summarized in Table 3. The S1−Tb concentration is held constant, and as the R6G concentration is reduced, the long lifetime component increases in both magnitude and fraction of overall lifetime.

Representative decay spectra and the associated intensity decay curves obtained from the same films are shown in Figures 5 and 6, respectively. Because the gated CCD camera collects the entire luminescence spectrum as a function of time, decay curves for different emission lines are obtained simultaneously. The lifetime of the 491 nm Tb emission is used to quantify energy transfer, and the results of fitting to these decay curves are summarized in Table 4.

Discussion

1. Mesostructure. The diffraction patterns for the mesostructured films shown in Figure 1 are representative of all the nanostructured thin films prepared as described in the Experimental Section. They are consistent with hexagonally packed arrays of cylindrical CTAB micelles.[1,23−25] The 2θ values of

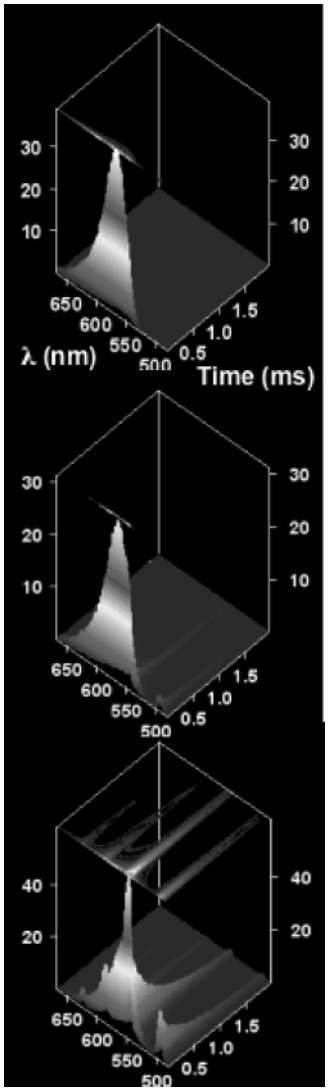

Figure 5. Decay spectra obtained from mesostructured thin films containing S1−Tb and R6G at R6G:Tb ratios of 20:100 (top), 6.7:100 (middle), and 1.6:100 (bottom). As the R6G concentration decreases, Tb quenching is reduced, and the characteristic Tb lines become more prominent. The spectra also show a microsecond lifetime for R6G, consistent with fluorescence lifetime measurements (Figure 4) made on R6G luminescence in the same films.

the peaks, and hence the lattice spacings (39.8 ± 0.7 Å), are the same for all samples within experimental error. The nature and concentrations of the dopants have no detectable effect on the nanostructure as assessed by XRD. Furthermore, the patterns for all doped films are identical, within experimental uncertainty, to those obtained from undoped films.

2. Deliberate Placement and Spatial Segregation. The syntheses employed here exploit two of the three strategies demonstrated previously[5,13,15] for deliberately placing molecules in different regions of the nanostructured thin films in a one-step process. The strategies derive from the properties that are particular to each of the three regions: the silicate framework, the hydrophobic region inside the micelles, and the ion-rich region composed of the surfactant heads and unreacted silanol groups at the interface between the framework and hydrophobic region. These regions are illustrated in Figure 1, and the

(23) Grosso, D.; Babonneau, F.; Albouy, P.-A.; Amentisch, H.; Balkenende, A. R.; Brunet-Bruneau, A.; Rivory, J. *Chem. Mater.* **2002**, *14*, 931−939.
(24) Habuchi, S.; Kim, H.-B.; Kitamura, N. *J. Photochem. Photobiol., A:* **2000**, *133*, 189−196.
(25) Huo, Q.; Margolese, D.; Stucky, G. D. *Chem. Mater.* **1996**, *8*, 1147−1160.

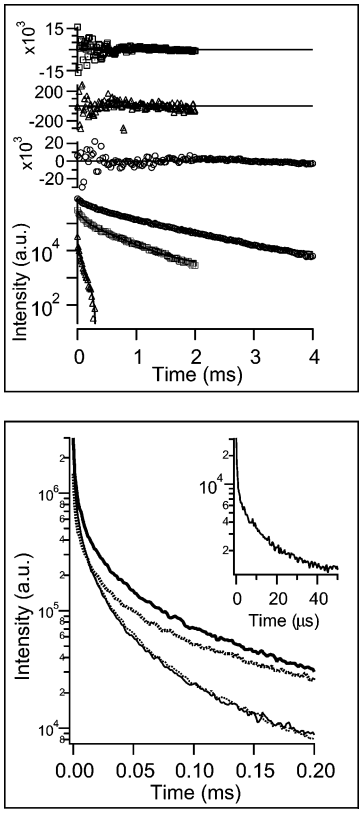

Figure 6. Luminescence decay curves obtained from the decay spectra shown in Figure 5. The top panel shows the decay curves for the Tb 491 nm emission line in the absence of R6G in an amorphous film (circles), with R6G in an amorphous film (squares), and with R6G in a structured film (triangles) at R6G:Tb = 20:100. The top traces are the residual plots. The bottom panel shows the decay curves for R6G emission from mesostructured films at R6G:Tb = 50:100 (solid line), 20:100 (dotted line), 6.7:100 (thick solid line), and 1.6:100 (thick dotted line). The data are in good agreement with FD lifetimes, which show that the long lifetime component comprises a larger fraction of the R6G lifetime at low R6G:Tb ratios. The inset is the decay curve from a structured film without Tb. In the absence of Tb, the unsensitized R6G fluorescence lifetime is shorter than the laser pulse width (10 ns).

strategies that target them are termed philicity, bonding, and bifunctionality.

Philicity is a manifestation of the propensity for molecules of similar physical characteristics to agglomerate when surrounded by an environment that has different physical properties as, for example, hydrophobic molecules do in water. In the context of nanostructured thin films, philicity operates by placing hydrophobic organic molecules inside the surfactant micelles. Such confinement of organic dyes has been shown for nonpolar molecules such as pyrene,[1] *p*-terphenyl,[13] a terrylene derivative,[13] and carbazole.[2] Surprisingly, polar molecules such as coumarin 540A[13] and salts such as rhodamine 700[26] and R6G also concentrate in the micelle, *vide infra*. The philicity strategy may take other forms: a fluorophore derivatized with a long alkyl chain being incorporated into micelles,[27−29] an ionic biomolecule preferring an interfacial position,[30] or a polar molecule taking up residence in the polar environs of the silicate framework.

The bonding strategy involves the chemical bonding of a dopant to the silicate framework. Previous studies and this work employ a lanthanide ligand that contains two trialkoxysilane groups that can cocondense with the silicate precursor (TEOS, in this case) to form the silicate framework.[5,21] When three ligands bind to each lanthanide, six trialkoxysilyl groups per metal complex react with TEOS to become part of the silicate framework.

In the following sections, the locations of the laser dye and the lanthanide complex are discussed. Steady-state luminescence spectra, FD lifetime data, TD lifetime data, and the Förster model for energy transfer are considered together to show that the two components are spatially separated from each other in two different regions of the thin films, that the distance between the two can be systematically altered by changing their concentrations, and that there are limits on how close to and how far from each other the two components may be placed.

3. R6G Location and Concentration Quenching. Data obtained from steady-state fluorescence spectra, excitation spectra, and fluorescence lifetime experiments show that R6G is associated with the CTAB micelles. The fact that both the fluorescence and the fluorescence excitation maxima in the visible region for R6G in structured films are each red shifted relative to the same maxima in amorphous films provides evidence that R6G resides in the CTAB micelles of nanostructured thin films.[9,31] These red shifts are consistent with R6G going from a polar environment to a nonpolar environment;[32−36] the nonpolar environment in the mesostructured material is the interior of the CTAB micelles. These observations are consistent with the documented behavior of R6G in concentrated solutions with and without surfactant.[33,34]

The higher fluorescence intensity of R6G in nanostructured films relative to amorphous films shows that the presence of CTAB affects R6G luminescence.[9,33,34] In the course of obtaining fluorescence spectra, it was noted that the fluorescence intensity obtained from nanostructured films containing R6G increases with increasing R6G concentration, reaches a maximum at R6G:CTAB = 24:1000, and then decreases as the R6G concentration increases further. This behavior is consistent with R6G concentration quenching, which is a well-documented phenomenon in dyes[37] and R6G in particular.[9,33−36,38−41]

Concentration quenching results from homotransfer (energy transfer from one R6G molecule to another one) at moderate dye concentrations and from aggregation at high concentrations. Both phenomena affect the fluorescence yield and lifetime of R6G at high concentrations, but aggregation is the major cause

(26) Minoofar, P. Doctoral Dissertation, University of California, Los Angeles, 2004.
(27) Gaines, G. L. *Inorg. Chem.* **1980**, *19*, 1710−1714.
(28) el Torki, F. M.; Schmehl, R. H.; Reed, W. F. *J. Chem. Soc., Faraday Trans. 1* **1989**, *85*, 349−362.
(29) Tavernier, H. L.; Laine, F.; Fayer, M. D. *J. Phys. Chem. A* **2001**, *105*, 8944−8957.
(30) Nguyen, D. Doctoral Dissertation, University of California, Los Angeles, 2003.
(31) Wirnsberger, G.; Stucky, G. *Chem. Mater.* **2000**, *12*, 2525−2527.
(32) Renge, I. *J. Phys. Chem. A* **2000**, *104*, 7452−7463.
(33) Jones, G. Photochemistry of Laser Dyes. In *Dye Laser Principles with Applications*; Duarte, F. J., Hillman, L. W., Eds.; Academic Press: San Diego, 1990; pp 287−335.
(34) Drexhage, K. H. Structure and Properties of Dye Lasers. In *Dye Lasers*; Schafer, F. P., Ed.; Springer-Verlag: Berlin, 1990; Vol. 1, pp 155−185.
(35) Bojarski, C.; Obermueller, G. *Acta Phys. Pol.* **1976**, *A50*, 389−411.
(36) Yuzhakov, V. *Russ. Chem. Rev.* **1979**, *48*, 2007−2033.
(37) Burdett, B. C.; Vitagliano, V. In *Aggregation Processes in Solution*; Wyn-Jones, E., Gormally, J., Eds.; Elsevier Scientific: Oxford, 1983; pp 241−307.
(38) Ghomashchi, E.; Ghanadzadeh, A.; Mahjani, M.; Hasanpour, M.; Niavaran, H. *Spectrochim. Acta* **1991**, *47A*, 211−217.
(39) Arbeloa, F.; Ojeda, P.; Arbeloa, I. *J. Photochem. Photobiol., A* **1988**, *45*, 313−323.
(40) Arbeloa, F.; Gonzalez, I.; Ojeda, P.; Arbeloa, I. *J. Chem. Soc., Faraday Trans. 2* **1982**, *78*, 989−994.
(41) Bojarski, P. *Chem. Phys. Lett.* **1997**, *278*, 225−232.

Table 4. Tb 491 nm Luminescence Lifetimes (τ_i, ms) in the Presence of R6G, Quenching Efficiency (% *E*), and Calculated Tb−R6G Distances (*R*, Å) in Mesostructured Thin Films[a]

R6G:Tb	type	% τ_1	τ_1 (ms)	% τ_2	τ_2 (ms)	% τ_3	τ_3 (ms)	% τ_4	τ_4 (ms)	$\langle\tau\rangle$	% *E*	R^b (Å)
0:100[c]	amorphous	92.1	0.76	7.9	0.11					0.71		
1.6:100	structured	87.9	0.83	11.3	0.18	0.8	0.021			0.75	<5[d]	>65
6.7:100	structured	75.2	0.69	22.2	0.14	2.6	0.017			0.55	29.5	46.3
20:100	structured			49.9	0.16	45.3	0.032	4.8	0.0042	0.097	87.8	28.8
50:100	structured			28.3	0.25	53.1	0.030	18.6	0.0044	0.087	89.1	28.2

[a] Average lifetimes $\langle\tau\rangle$ and lifetime percentages are calculated according to eqs 2 and 3, respectively. Standard deviations for lifetime percentages and lifetimes are $\sigma \leq 5\%$. [b] *R* is calculated according to eq 5. [c] The lifetime at R6G:Tb = 0:100 is the average value from amorphous films obtained from each sol prior to addition of R6G. [d] There was little donor quenching in this instance. The values reported are the upper limit on quenching and the lower limit on the D−A separation.

for concern in energy transfer studies and distance measurements according to the Förster model because R6G aggregates have spectral properties different from those of R6G "monomers".[36,38−40] Consequently, aggregation in the films was studied in detail.

To determine the concentration at which R6G aggregation occurs in nanostructured thin films, the FD fluorescence lifetime of R6G is measured in structured thin films with different R6G:CTAB ratios. (The ratios are evaluated for the starting sol and are assumed to be retained during film formation.) The data, summarized in Table 1, show the onset of concentration quenching at an R6G:CTAB concentration ratio of approximately 24:1000. When the ratio exceeds this value, a subnanosecond lifetime component comprises an increasingly larger fraction of the overall R6G lifetime as the R6G concentration increases, with the peak fraction of 70% occurring at R6G:CTAB = 50:1000 (Table 1). This result is an indication that concentration quenching is appreciable at R6G:CTAB > 24:1000. Reflectance absorbance spectra of the films showed an absorbance peak belonging to R6G aggregates only at R6G:CTAB = 50:1000, the highest R6G concentration. Hence, concentration quenching begins at R6G:CTAB = 24:1000, and aggregation becomes appreciable at higher R6G:CTAB ratios. Therefore, the distance measurements discussed in section 5 are valid only for films in which the R6G:CTAB ratio is less than 24:1000, the regime where the subnanosecond lifetime component comprises less than 30% of the overall R6G lifetime and no evidence for aggregates is observed in reflectance spectra.

It is worthwhile to remark that the R6G:CTAB ratio of 24:1000 has a geometrical explanation given the average CTAB aggregation number of 90 in spherical aqueous micelles.[29,42−46] The experimentally determined hydrodynamic radius of 24.5 Å[44,45] for these micelles can be used to calculate the number of CTAB molecules that comprise a cross section of such micelles by calculating how many cones of CTAB's reported dimensions[44−46] can fit in a sphere of radius 24.5 Å. This calculation yields 10 CTAB molecules per micellar cross-section. Using this value, at R6G:CTAB = 24:1000 there is one R6G molecule for every four CTAB cross sections in the cylindrical micelles, and R6G molecules are on average no further than 20 Å apart at this R6G:CTAB ratio. At such short distances homotransfer becomes probable.[24,39] The effect of this transfer is manifested in the fast lifetime component that appears at R6G:CTAB = 24:1000. The fraction of the overall lifetime that this fast component represents increases monotonically with R6G concentration, and at R6G:CTAB = 50:1000 its 70% share of the overall lifetime suggests that aggregates are the dominant species in the micelles. Hence, the R6G:CTAB ratio of 24:1000 may be regarded as the aggregation threshold. Because the foregoing explanation relies solely on the size of R6G relative to the micelle dimensions involved, dyes similar in dimensions to R6G would be expected to have the same aggregation threshold in CTAB templated films, as has been found with rhodamine 700[26] and pyrene.[47]

4. Lanthanide Location. The sensitivity of the lanthanide luminescence lifetimes,[48−52] and that of the Eu luminescence lifetime in particular,[50−55] has been used to characterize the immediate environment of the lanthanide. Previous reports[5,13] exploited this sensitivity to show that the environment of lanthanide complexes with organic ligands in amorphous films is different from their environment in structured films; complexes in structured films had a lifetime that was 10% longer than that in amorphous films. The same studies also showed that structurally similar lanthanide complexes with alkoxysilylated ligands have the same environment in both types of film. The apparently constant environment of lanthanides bound to the alkoxysilylated ligands suggested that these complexes are localized in the silicate framework. Parallel studies with Eu bound alternately to PyDCA or S4 (Chart 2) are reported here, and the data are in agreement with previous accounts. Luminescence lifetime results are summarized in Table 2.

The data show that when the fully ligated Eu is bound to the silylated ligand S4 (Eu:S4 = 1:6), the luminescence lifetime for both the long and short lifetime components are the same in both amorphous and structured films. In contrast, when Eu is bound to the PyDCA, the lifetime in structured films is different (10% longer for the long lifetime component and 50% for the short lifetime component) from that in amorphous films. In the cases of stoichiometries where all of the lanthanide ions

(42) Nagarajan, R. *Langmuir* **2002**, *18*, 31−38.
(43) Tanford, C. *J. Phys. Chem.* **1972**, *76*, 3020−3024.
(44) Roelants, E.; De Schryver, F. C. *Langmuir* **1987**, *3*, 209−214.
(45) Weidemaier, K.; Tavernier, H. L.; Fayer, M. D. *J. Phys. Chem. B* **1997**, *101*, 9352−9361.
(46) van Os, N.; Haak, J.; Rupert, L. *Physico-Chemical Properties of Selected Anionic, Cationic and Nonionic Surfactants*; Elsevier: Amsterdam, 1993.
(47) Forster, T.; Selinger, B. *Z. Naturforsch.* **1964**, *19a*, 38−41.
(48) Goncalves e Silva, F. R.; Malta, O. L.; Reinhard, C.; Gudel, H.-U.; Piguet, C.; Moser, J.; Bunzlie, J.-C. G. *J. Phys. Chem. A* **2002**, *106*, 1670−1677.
(49) Bruno, J.; Horrocks, W. D.; Zauhar, R. *Biochemistry* **1992**, *31*, 7016−7026.
(50) Sabbatini, N.; Guardigli, M.; Lehn, J.-M. *Coord. Chem. Rev.* **1993**, *123*, 201−228.
(51) Choppin, G. R.; Peterman, D. R. *Coord. Chem. Rev.* **1998**, *174*, 283−299.
(52) Steemers, F. J.; Verboom, W.; Reinhoudt, D. N.; van der Tol, E. B.; Verhoeven, J. W. *J. Am. Chem. Soc.* **1995**, *117*, 9408−9414.
(53) Silversmith, A. J.; Boye, D. M.; Anderman, M. T.; Brewer, K. S. *J. Lumin.* **2001**, *94−95*, 275−278.
(54) Park, Y. J.; Lee, B. H.; Kim, W. H.; Do, Y. *J. Colloid Interface Sci.* **1999**, *209*, 268−270.
(55) Albin, M.; Whittle, R. R.; Horrocks, W. D. *Inorg. Chem.* **1985**, *24*, 4591−4594.

are not fully ligated (Eu:ligand = 2:3), comparisons become more difficult because of multiple species present in the films. However, for the silylated ligand complex, the two major components again have the same lifetimes in both the structured and amorphous films, but in the PyDCA complex the predominant species (>97%) has different lifetimes in the structured and amorphous films. The equality of the lifetimes of the silylated complex in the two different films shows that it is bound to the silica in both cases; the lifetime differences for the complex that cannot bind suggest that it resides in different regions in the two different films (in the surfactant region in structured films and in the silica in amorphous films).

5. Energy Transfer from Tb to R6G. The films that were prepared for energy transfer studies all contained the same concentration of the S1−Tb complex (Si:S1:Tb = 117:3:1 in the starting sol). The concentration of R6G was varied to produce films with R6G:Tb concentration ratios of 1.6:100, 6.7:100, 20:100, and 50:100. One film in which the R6G concentration exceeded the aggregation threshold established in section 3 above is included for comparison (R6G:Tb = 50:100). In all other instances, the R6G concentration was below the aggregation threshold in CTAB.

Steady-state luminescence spectra, FD lifetime measurements of R6G luminescence, and lifetime measurements on Tb 491 nm emission provide definitive evidence for energy transfer. The Tb luminescence lifetime measurements are used to calculate the distance between Tb and R6G in nanostructured films according to the Förster model. The Tb 491 nm decay curves fit adequately to decay laws predicted for nonrandomly distributed ensembles of donors and acceptors.

A. Luminescence and Luminescence Lifetimes. Luminescence spectra and luminescence lifetimes of R6G verify that energy transfer from Tb to R6G occurs. The steady-state luminescence spectra and photoexcitation spectra show two signs of energy transfer. Luminescence spectra excited at the absorption maximum of the Tb ligand show enhanced R6G emission in films with Tb relative to the emission of films without Tb. Enhanced, or sensitized, R6G emission is observed in all films containing Tb at all concentrations of R6G. Accordingly, the Tb emission intensity is reduced dramatically in the presence of R6G. This quenching of Tb luminescence shows a strong dependence on R6G concentration, and all Tb emission lines are quenched equally, with no selective reduction in intensity.

In a complementary experiment, the photoexcitation spectra for R6G show a new peak in the ultraviolet region when the Tb complex is present (Figure 3). The position of the new peak corresponds exactly to the Tb complex's photoexcitation maximum (Figure 3, bottom panel). The appearance of this peak in the photoexcitation spectra of R6G proves that energy transfer occurs because it clearly establishes the dependence of R6G fluorescence on the Tb complex's absorbance. As the bottom panel of Figure 3 shows, at low R6G concentration (R6G:Tb = 1.6:100) the R6G intensity obtained from 276 excitation is very large (and rivals that obtained from 530 nm excitation) even though the extinction coefficient of R6G is much lower at 276 nm. Given the fact that the components are dispersed in uniform films less than 2000 Å thick, this finding cannot be explained by other mechanisms such as inner filtering and firmly establishes energy transfer as the dominant mechanism of Tb quenching by R6G.

Fluorescence lifetime measurements carried out on R6G luminescence confirm this conclusion. The data, depicted in Figure 4 and summarized in Table 3, show that R6G luminescence lifetime increases as much as 3 orders of magnitude (to 1.55 μs) in the presence of the Tb complex. Both the magnitude of this long lifetime component and the fraction of the overall lifetime that it comprises increase as the R6G content *decreases*. At high R6G content, energy transfer is efficient because donors and acceptors are close to each other, and consequently, the supply of excited Tb donors is rapidly depleted by the large number of nearby R6Gs. At low R6G content, the donors and acceptors are far apart, and the supply of excited Tb is exhausted over a longer time; thus, the sensitized R6G luminescence comprises a larger fraction of the overall R6G lifetime (and R6G luminescence). As Table 4 shows, the complementary effects are observed in the Tb luminescence lifetimes: when the R6G concentration is high, the Tb lifetime is short, and vice versa.

B. Distance Measurements. This section describes the experiments that were carried out and the assumptions that were made to calculate the various quantities in the Förster model of energy transfer[22,56] that are used to calculate the distance between Tb and R6G in the nanostructured films. The model describes energy transfer as the coupling of electron transition dipoles acting on transitions of equal energy in the donor and acceptor. This assumption leads to the following expression for the probability of energy transfer, k:

$$k = \frac{1}{\tau_D}\frac{1}{R^6}\frac{9000(\ln 10)\kappa^2\phi_D}{128\pi^5 n^4 N}\int F_D(\lambda)\,\epsilon_A(\lambda)\,\lambda^4\,d\lambda \qquad (4)$$

$$k = \frac{1}{\tau_D}\frac{R_o^{\,6}}{R^6} \qquad (5)$$

where n is the refractive index of the medium, κ^2 is the orientation factor resulting from the vector nature of dipole transitions, N is Avogadro's number, ϕ_D is the donor quantum yield, $F_D(\lambda)$ is donor (Tb) emission (normalized to unity) as a function of wavelength, λ, ϵ_A is the extinction coefficient of the acceptor (R6G), and R is the distance between the donor and acceptor. The collection of constants and the integral are subsumed into the term R_o^6. The term R_o is called the Förster radius, has the units of distance, and is unique for each donor−acceptor pair. The Förster model has been used to calculate distances between donor−acceptor pairs consisting of lanthanides and organic dyes.[57−59]

The UV−vis absorption spectrum of an ethanolic R6G solution of known concentration and an emission spectrum of the terbium complex (Figure 2) are used to calculate the spectral overlap integral in the rate expression. The resulting calculated spectral overlap, $J = \int F_D(\lambda)\,\epsilon_A(\lambda)\,\lambda^4\,d\lambda = 3.07 \times 10^{15}$, is large and is similar to the overlap calculated for other systems consisting of a lanthanide donor and an organic acceptor.[59−61] The orientation of the dipoles with respect to each other is assumed to be random, yielding an orientation factor, κ^2, of 2/3.

(56) Forster, T. *Discuss. Faraday Soc.* **1959**, *27*, 7−17.
(57) Selvin, P. R. *Methods Enzymol.* **1995**, *246*, 300−334.
(58) Selvin, P. R. *IEEE J. Sel. Top. Quantum Electron.* **1996**, *2*, 1077−1087.
(59) Root, D. D.; Stewart, S.; Xu, J. *Biochemistry* **2002**, *41*, 1786−1794.
(60) Selvin, P. R.; Rana, T. M.; Hearst, J. E. *J. Am. Chem. Soc.* **1994**, *116*, 6029−6030.
(61) Root, D. D.; Shangguan, X.; Xu, J.; McAllister, M. A. *J. Struct. Biol.* **1999**, *127*, 22−34.

The refractive index, n, is estimated as follows. The CTAB lattice spacing obtained from the CTAB powder XRD pattern is 25 Å. CTAB is assumed to contribute the same distance to the observed lattice spacing of 40 Å in the thin films. This assumption leads to the conclusion that the thickness of the silicate framework is approximately 15 Å. Hence, because the medium between Tb and R6G is composed primarily of CTAB and the organic ligand, the index of refraction of hexadecylamine, $n = 1.44$, was used.[62]

The quantum yield, ϕ, of the Tb donor in the mesostructured films was estimated to be 0.15 by using the relationship $\phi = \tau/\tau_i$,[59,63] where τ_i is the intrinsic lifetime of the Tb excited state. Using the previously reported value of $\tau_i = 4.75$ ms[61,64] and an average lifetime of 0.7 ms measured for Tb in thin films, a value of $\phi_D = 0.15$ is calculated. This estimate is probably accurate to ± 0.05 given the variations measured in Tb lifetimes. Inserting values of 10% and 20% for the quantum yield into the expression for the Förster radius gives the boundaries of 35 and 45 Å, respectively. It is interesting to note that this value of 40 Å is close to that of the tube center to framework center distance of about 20 Å. (CTAB tubes have a radius of about 12 Å, the framework is approximately 20 Å thick, and the lattice spacing is $d = 39.8$ Å.)

i. Distance between Tb and R6G. The donor and acceptor are separated in space in the different regions of the nanostructured thin films: R6G in the micelles and the Tb complex in the silicate framework. To use the Förster model to calculate the separation between the two, the Förster radius must be on the same order as the distance from the center of the hydrophobic region inside the micelles to the center of the silicate framework. This distance is about 20 Å, half of the d spacing calculated from the first-order diffraction peak in the XRD pattern. The calculated Förster radius of 40 Å makes the Tb−R6G system suitable for this analysis.

Efficiency of energy transfer, E, is calculated by inserting the weighted average lifetime of the 491 nm Tb luminescence line at different R6G concentrations and the average lifetime for the amorphous film containing S1−Tb only into eq 6,

$$E = \frac{R_o^6}{R^6 + R_o^6} = 1 - \frac{\tau_{DA}}{\tau_D} = 1 - \frac{F_{DA}}{F_D} \qquad (6)$$

where E is the calculated quenching efficiency, τ_D and F_D are the lifetime and fluorescence intensity of the donor in the absence of acceptor, and τ_{DA} and F_{DA} are the corresponding quantities in the presence of acceptor.[22,56] The calculated Förster radius and the experimentally obtained quenching efficiencies are used to solve eq 6 for R, the donor−acceptor distance. The results are summarized in Table 4.

The Tb−R6G distance decreases as the R6G concentration is increased. At the lowest R6G concentration, R6G:Tb = 1.6:100, a small quenching of 5% is measured, corresponding to a large Tb−R6G distance of $R = 65$ Å. This distance decreases as the R6G concentration increases until it reaches a value of 29 Å at R6G:Tb = 20:100. When the R6G content is more than doubled to R6G:Tb = 50:100, the Tb−R6G distance remains the same, within experimental error. This surprising result is probably caused by R6G aggregation in the micelles at high R6G concentrations. The study of R6G aggregation in nanostructured films, discussed in section 3, showed that aggregation becomes important at R6G:Tb = 50:100. Because the R6G concentration is higher than the aggregation threshold in this film, the implication is that the excess of R6G beyond the aggregation threshold is consumed entirely by aggregates whose different spectral properties lead to less efficient quenching of the excited Tb center.

A different perspective of the trends is obtained by focusing on the number of Tb complexes that donate to R6G. The number of Tb donors is in excess of the number of R6G acceptors; as more R6G is added, the total number of Tb donors that can undergo energy transfer increases. The result is an apparent increase in energy transfer efficiency and an apparent decrease in donor−acceptor separation. Thus, as the amount of R6G is increased the incidents of energy transfer increase until the threshold is reached when all of the Tb donors undergo energy transfer. The distance calculated at this threshold is 28 Å. An interesting aspect of this view of the results is that the distance between the donors and acceptors is fixed by the structure of the material, and the efficiency for a given donor toward its nearest acceptor does not change by a large amount (the lifetime changes are less than 10% in τ_1), but the number of molecules undergoing FRET increases (as shown by the decrease in the preexponential factor).

The unifying feature of the focus on average distances and the focus on number of donors quenched is the average distance between the donor and acceptor. It is important to emphasize that the analysis measures average distances. There is no strict correlation between these measured distances and the distribution of distances and, consequently, no implication that energy transfer becomes more efficient at higher R6G concentrations (i.e., that all Tb−R6G distances are getting reduced). As the arrangement of lifetimes in Table 4 shows, the increase in observed quenching efficiency reflects the increasing probability of finding an R6G molecule within one Förster radius of Tb. At low R6G concentrations (up to R6G:Tb = 6.7:100), the magnitude of τ_1 does not change significantly. Rather, it comprises a smaller fraction of the overall lifetime. As the fraction of τ_1 decreases and eventually vanishes, the fractions of τ_2 and τ_3 increase, and a very short lifetime, τ_4, appears. The long lifetime is clearly characteristic of unquenched Tb centers, and the shorter lifetimes are unmistakably attributed to Tb quenched by ever closer R6G molecules. It is more accurate, therefore, to say that at higher R6G concentrations the probability of finding an R6G within effective quenching distance of Tb is higher (rather than quenching efficiency is a reflection of more effective quenching). The shortest lifetime, τ_4, may be a result of R6G aggregation.

ii. Nonrandom Distribution. The two-dimensional hexagonal structure of the films implies that the donor and acceptor could be distributed in a nonrandom manner in the nanostructured sol−gel thin films. To test this implication, an attempt was made to examine whether Tb luminescence decays in the presence of R6G conformed to laws predicted by the theories that govern energy transfer between nonrandomly distributed populations of donors and acceptors.[22,65−69] This is a subject of significant

(62) *The Merck Index*, 13th ed.; Merck and Co./CambridgeSoft Corp.: Cambridge, 2002.
(63) Xiao, M.; Selvin, P. R. *J. Am. Chem. Soc.* **2001**, *123*, 7067−7073.
(64) Stein, G.; Wurzberg, E. *J. Chem. Phys.* **1975**, *62*, 208−213.
(65) Levitz, P.; Drake, J. M.; Klafter, J. *J. Chem. Phys.* **1988**, *89*, 5224−5236.
(66) Tcherkasskaya, O.; Klushin, L.; Gronenborn, A. M. *Biophys. J.* **2002**, *82*, 988−995.
(67) Blumen, A. *J. Phys. Chem.* **1981**, *74*, 6926−6933.

complexity, and it will not be discussed at length here because, with one exception, none of the decay curves fit the predicted decay pattern for a nonrandomly distributed ensemble of donors and acceptors of fewer than three dimensions.

The theory averages decay patterns arising from a collection of self-similar units, or fractals, consisting of donors and acceptors arranged in a particular geometry. If as a result of nonrandom distribution these fractals have fewer than three dimensions, the reduced dimensionality may be deduced experimentally from the fractional exponent $n/6$ in a "stretched" exponential similar to

$$\boldsymbol{I}(t) = A_1 \exp\left[-\frac{t}{\tau_1} - \gamma\left(\frac{t}{\tau_1}\right)^{n/6}\right] + A_2 \exp\left(-\frac{t}{\tau_2}\right) \quad (7)$$

where $n = 1$, 2, or 3 for fractals with one, two, or three dimensions, respectively. The lifetime decays obtained for Tb in nanostructured films were fit to eq 7 to see whether the decay curves conformed to ensemble averages predicted for nonrandomly distributed donor−acceptor populations. This analytical expression was derived in the references cited and applied previously to D−A assemblies obtained in Langmuir−Blodgett films.[70]

Because the restricted geometry that results from the confinement described here has fewer than three dimensions, an n value that is between 2 and 3 is expected. However, if the ensemble consists of too many repeat units, the average converges to the three-dimensional limit regardless of fractal dimensions. Furthermore, the derivations are valid for fixed donor to acceptor distances, not for distributions of these distances.[22,66,69]

Statistically adequate fits of the Tb 491 nm luminescence lifetime to eq 7 were obtained for all mesostructured films. The resulting values of n were 3.2, 3.3, and 3.2 when the R6G:CTAB mole ratios were 1.6:100, 6.7:100, and 20:100, respectively. These results are interpreted as a nonrandom distribution of donors and acceptors composed of three-dimensional fractals. A value of 2.6 is obtained for n at R6G:Tb = 50:100, a R6G concentration at which aggregation in CTAB has been documented by both FD lifetime measurements and visible absorption. A possible reason the fractional exponent converges to a value characteristic of reduced dimensionality of the donor−acceptor distribution at high R6G concentration is that R6G aggregation in CTAB micelles acts as an additional constraint on the R6G monomer distribution that sharpens the donor−acceptor distance distribution. The reduced dimensionality of such a system has been suggested before.[17]

Summary

Silicate thin films with highly ordered nanostructure containing spatially separated luminescent molecules are synthesized. The films consist of a silicate framework that holds in place a two-dimensional hexagonal structure with a lattice spacing of 40 Å templated by an ionic surfactant. Pairs of molecules consisting of an energy donor lanthanide complex and an energy acceptor rhodamine dye are placed in the framework and the surfactant, respectively, using a recently developed one-step one-pot synthesis. The lanthanide complex contains silylated ligands that bond to and form part of the framework, and that are an example of the "bonding" strategy for deliberate placement. The rhodamine dye is localized in the hydrophobic region of the surfactant, and its placement is an example of the "philicity" strategy. The films, deposited on a silicon substrate, are smooth within a quarter wavelength of visible light, transparent, and stable.

The spectroscopic data show that R6G is incorporated into the surfactant micelles and that lanthanide complexes involving the alkoxysilylated ligands shown in Charts 1 and 2 are incorporated into the silicate framework of mesostructured thin films. The more intense (by more than an order of magnitude) and red-shifted peaks in the fluorescence and photoexcitation spectra of R6G in mesostructured films relative to those in the spectra in amorphous films demonstrate that R6G is incorporated into the surfactant micelles of mesostructured thin films. The manifestation of concentration quenching and aggregation in fluorescence spectra and fluorescence lifetime measurements in mesostructured thin films demonstrate that even large R6G concentrations are incorporated into the CTAB micelles. When the lanthanide's ligand is not silylated, the complex is incorporated in the surfactant region of the structured film. Its luminescence lifetime is different from that in an unstructured (pure silica) film where the complex is located in the silica. In contrast, when the ligand is silylated and forms the silica framework, the lifetime is the same as that when the complex is in the pure silica film. These results show that the silylated ligands' ability to react with TEOS incorporates the lanthanide complex into the silicate framework.

Quantitative studies of energy transfer between Tb and R6G in the mesostructured films are used to calculate the distance between the donor and acceptor. Steady-state fluorescence and photoexcitation spectra, R6G fluorescence lifetimes, and Tb luminescence lifetimes show that excited Tb complexes transfer their energy to nearby R6G molecules in a concentration-dependent manner. The excitation spectra show that absorption of light by the lanthanide complex results in emission of light from the R6G. The lifetime of the lanthanide complex decreases and that of R6G increases. Quantitation of the data according to Förster theory shows that the separation between Tb and R6G can be large enough at low concentrations to reach the limit where nearly no quenching occurs (∼65 Å) but that it gets no smaller than ∼29 Å at high R6G concentrations.

This study demonstrates self-assembly of spatially separated donor and acceptor molecules in a transparent nanostructured optically transparent continuous thin film. The preparation strategies are simple and expandable to a wide variety of donor and acceptor molecules for both photoinduced energy transfer (as demonstrated in this paper) and electron transfer.

Acknowledgment. This work was supported by NSF Research Grant DMR-0103952 and Instrument Grant DMR-0114002. We acknowledge undergraduate students Amy Durisin and Justin Glover for assistance in the synthesis of films and acquisition of data, and Professor Robert N. Schwartz for helpful discussions. We thank a reviewer for additional insight into the interpretation of the distances obtained from the energy transfer data.

JA045185E

(68) Clegg, R. M. *Curr. Opin. Biotechnol.* **1995**, *6*, 103−110.
(69) Baumann, J.; Fayer, M. D. *J. Chem. Phys.* **1986**, *85*, 4087−4107.
(70) Jensen, K. K.; Albinsson, B.; Van der Auweraer, M.; Vuorimaa, E.; Lemmetyinen, H. *J. Phys. Chem. B* **1999**, *103*, 8514−8523.